JMEPEG (2018) 27:282–292
https://doi.org/10.1007/s11665-017-3019-6

1059-9495/$19.00

Vacuum Pressureless Sintering of Ti-6Al-4V Alloy with Full Densification and Forged-Like Mechanical Properties

Ce Zhang, Boxin Lu, Haiying Wang, Zhimeng Guo, Vladislav Paley, and Alex A. Volinsky

(Submitted June 15, 2017; in revised form September 17, 2017; published online December 18, 2017)

Ti-6Al-4V ingots with a nearly 100% density, fine and homogeneous basket-weave microstructure, and better comprehensive mechanical properties (UTS = 935 MPa, Y.S. = 865 MPa, El. = 15.8%), have been manufactured by vacuum pressureless sintering of blended elemental powders. Coarse TiH_2 powder, Al powder (2, 20 μm), V powder, and Al-V master alloy powder were used as raw materials to produce different powder mixtures (D_{50} = 10 μm). Then, the compacts made by cold isostatic pressing were consolidated by different sintering curves. A detailed investigation of different as-sintered samples revealed that a higher density can be obtained by generating transient molten Al in the sintering process. Coarse Al powder and a rapid heating rate under the melting point of Al contribute to molten Al formation. The presence of temporary liquid phase changes the sintering mechanism, accelerating the sintering neck formation, improving sinterability of the powder mixtures. Density of 99.5% was achieved at 1150 °C, which is markedly lower than the sintering temperatures reported for conventional blended elemental powder metallurgy routes. In addition, low interstitial content, especially for oxygen (0.17 wt.%), is obtained by strict process control.

Keywords full density, mechanical properties, microstructure, Ti-6Al-4V, vacuum sintering

1. Introduction

Titanium and its alloys are ideal materials for many industries due to unique low density, high strength and fracture toughness, good corrosion resistance, and biocompatibility. However, titanium use is far less widespread relative to other structural metals (i.e., steel or aluminum). Exceptions are limited to high-tech industries, like aircraft, spacecraft, and biomedical applications due to Ti high extraction and production costs (Ref 1-5). Now, the traditional technique for high-performance Ti alloys is as follows: titanium sponge → vacuum melting → as-cast Ti ingot → multiple forging → as-forged Ti ingot → heat treatment → machining → components. Among these processes, the key technology for producing high-quality Ti alloys is wrought material processing. However, as-forged Ti alloys are quite expensive for most commercial applications (Ref 6). Because of this, powder metallurgy (PM) has long been regarded as a promising method to reduce the cost of Ti alloys, owing to its near-net-shape capabilities, more uniform and homogenous microstructure, and isotropic properties (Ref 7). This means that Ti and Ti alloy ingots can be produced from titanium sponge by PM methods, instead of the complicated vacuum melting and forging processes.

Ce Zhang, Boxin Lu, Haiying Wang, and **Zhimeng Guo**, Institute of Advanced Materials and Technology, University of Science and Technology Beijing, Beijing 100083, People's Republic of China; and **Vladislav Paley** and **Alex A. Volinsky**, Department of Mechanical Engineering, University of South Florida, Tampa, FL 33620. Contact e-mails: zmguo@ustb.edu.cn and volinsky@usf.edu.

Specific to Ti PM, the most pressing task is seeking a way to achieve comprehensive mechanical properties, which can match as-forged Ti alloys, while keeping the cost low. Currently, numerous studies have focused on Ti production components by PM methods, attempting different combinations of powders and sintering processes. There are two representative processing routes for PM Ti.

The first one is pre-alloyed (PA) powder with pressure-assisted sintering. The PA Ti alloy powder is produced by gas atomization, plasma rotating electrode process, or various other techniques. These processes yield the same chemical composition of the Ti alloys. Subsequently, pressure-assisted sintering processes, such as hot isostatic pressing, hot pressing, and spark plasma sintering, achieve nearly fully densified Ti alloys. This processing results in full density and improved mechanical properties similar to wrought alloys. However, the higher cost of PA powder and pressure-assisted sintering process, diminishes the advantages of PM processing.

The second process is blended elemental (BE) powder with pressureless sintering. To keep Ti PM cost down, one should only use low-cost powder, near-net-shape compaction, and the pressureless sintering processes. However, because of the porosity in the BE powder solidification during pressureless sintering, it is difficult to achieve relative density greater than 98%. Since sintering at elevated temperatures facilitates densification of the Ti alloy, a sintering temperature above 1300 °C is necessary to obtain high densification levels (Ref 8). In addition, higher temperature leads to grain coarsening, which is detrimental to the mechanical properties of Ti. Manufacturing Ti alloy with wrought-like mechanical properties through pressureless sintering of BE powder would be a breakthrough that could transform the Ti industry. Over the years, a few developments in BE technology have been made. The employment of the Hunter sponge fine powder (Ref 22), produced by the Armstrong process (ITP powder) (Ref 17, 23, 24), and hydrogenated Ti powder (Ref 25, 26), replaced hydrogen dehydrogenation (HDH) powder. Novel techniques, such as

Table 1 Mechanical properties of PM Ti-6Al-4V prepared by different processes

Process route	Relative density, %	Tensile strength, MPa	Yield strength, MPa	Elongation, %
Wrought (Ref 9)	~ 100	978	923	16
PAP + HIP (Ref 10-12)	~ 100	930-980	890-910	15-18
PAP + PCE (Ref 13, 14)	99	1300	1255	7.1
PAP + PCF (Ref 14, 15)	99	1450	1350	4.0
PAP + SPS (Ref 16)	99.5	901	NR	13.1
BEP + CP/CIP + VS (Ref 17, 18)	96	900	852	4
BEP + HSPT (Ref 19)	> 99	994-1024	930-974	13.8-17.8
BEP + ECAP + VS (Ref 20, 21)	> 99	1036-1069	917-954	7.8-13.1

PAP pre-alloyed powder, *BEP* blend element powder, *HIP* hot isostatic pressing, *CIP* cold isostatic pressing, *CP* cold pressing, *PCE* powder compact extrusion, *PCF* powder compact forging, *SPS* spark plasma sintering, *VS* vacuum sintering, *HSPT* hydrogen sintering and phase transformation, *ECPA* equal-channel angular pressing

equal-channel angular pressing (ECAP), hydrogen sintering and phase transformation (HSPT), and MR-9TM (Ref 27), were reportedly able to increase relative density of the products to achieve better mechanical properties. The mechanical properties of Ti-6Al-4V prepared by different PM processes are comparable with those of wrought Ti alloys, as shown in Table 1. However, relatively little attention has been paid to the traditional BE process, which is simple and practical for large-scale production of PM Ti alloys.

In this work, the wrought-like mechanical properties of Ti-6Al-4V ingots are achieved by combining conventional cold isostatic pressing and vacuum sintering. Density, microstructure, and mechanical properties were characterized, and the effects of microstructure on these properties were investigated. Different powder mixtures and sintering profiles were studied to understand the effects of molten aluminum. A transient liquid-phase sintering model is utilized to explain the high density obtained by a relatively low sintering temperature.

2. Experimental Procedure

The starting materials were TiH_2 powder with a 180-830 μm particle size (20-80 mesh), Al powder with two particle sizes (99.85% purity, D_{50} = 20 μm, D_{50} = 2 μm), and V powder (99.7% purity, D_{50} = 20 μm). A binary MA powder having a chemical composition of 60 wt.% of Al and 40 wt.% of V, was also used in this study.

Schematic illustration of the preparation process is shown in Fig. 1, where Powder I is the raw material. The as-received coarse TiH_2 powder was jar milled to crush and then sieved to a particle size below 20 μm, designated as Powder II. Subsequently, the Powders II and V were placed into a vacuum furnace, heated to 800 °C and held for 5 h. This achieved dehydrogenation and a homogeneous distribution of V through diffusion at the same time, designated as Powder III. Then, this powder and Al powder were weighed and combined in a sealed bottle to blend for 1 h, becoming Powder IV. Green compacts with relative 82.8 ± 0.6% density were prepared from Powder IV by compacting it at 200 MPa, using cold isostatic pressing (CIP) technique. For vacuum sintering, there were four thermal profiles used to produce Ti alloys, as shown in Fig. 1. Sintering profiles I-III had a rapid heating rate of > 10 °C/min, below Al melting point, but had different maximum temperature ranging from 1050 to 1250 °C. For comparison, sintering curve IV adopted a slow heating rate of < 5 °C/min, up to 1150 °C. As shown in Table 2, six samples were prepared by different powder mixtures and sintering curves in this study. It should be noted that all the powder handling was performed under N_2 protection to minimize oxidation. The sintering was performed under high vacuum of about 10^{-3} Pa.

The sintered samples' density (ρ_s) was measured using the Archimedes method according to the ASTM B328. The relative density values were calculated as $\rho_s/\rho_n \times 100$, where ρ_n is the nominal density of the Ti-6Al-4V alloy, found to be 4.43 g/cm^3. Room temperature tensile tests were conducted using the AGI-250 KN testing machine, at the strain rate of 1×10^{-3} s^{-1}, according to the ASTM E8-08. For each sample, five tensile test specimens were used to ensure results repeatability. Inductively coupled plasma atomic emission spectroscopy (ICP-AES) was used for bulk chemical analysis of the as-sintered samples. The phase composition of powders was analyzed by x-ray diffraction (XRD) using the Shimadzu XRD-6000 diffractometer with Cu Kα radiation operating at 40 kV and 40 mA between 30° and 80°. The interstitial elements (O, N, H) content in these samples was measured with the ELTRA ONH-2000 apparatus. Optical microscopy using the Axio Imager M2m and scanning electron microscopy using Philips LEO-1450 were used to examine the microstructure, fracture surfaces, and surface morphology of the powder. Differential scanning calorimetry (DSC) using EXSTAR 6000 was used to detect the presence of molten Al in the sintering powder compacts. Samples were heated to 800 °C at 15 °C/min and held for 15 min in high-purity argon flow.

3. Results and Discussion

3.1 Powder and Chemical Analysis

The starting materials in this study were coarse TiH_2 to reduce interstitial pickup, which were crushed to obtain fine TiH_2. The laser particle size distribution of Powders II-IV is about D_{10} = 4 μm, D_{50} = 10 μm, D_{90} = 17 μm. As shown in Fig. 2, both powders exhibit small particle size range, with an irregular shape, except for a little spherical Al powder denoted with white arrows. Cracks in the particles are commonly observed in Fig. 2(c), suggesting that this powder is produced by crushing brittle TiH_2. The XRD patterns of Ti-4V powder and pure Ti powder are shown in Fig. 3. Two main chemical

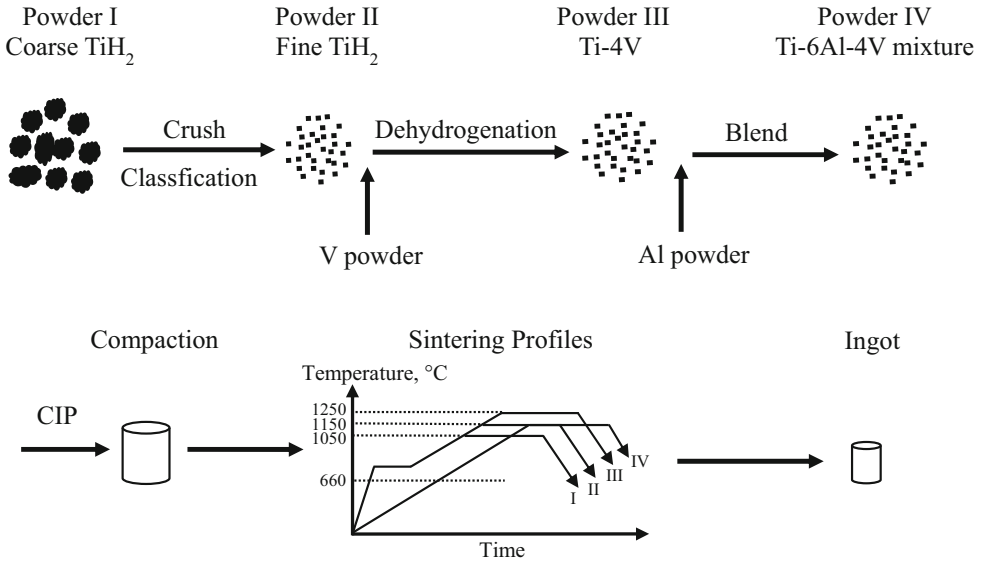

Fig. 1 Schematic illustration for the PM Ti-6Al-4V preparation process

Table 2 Powder mixtures and sintering profiles used to prepare the samples

Samples	#1	#2	#3	#4	#5	#6
Powder Mixtures	Powder III + C-Al	Powder III + C-Al	Powder III + C-Al	Powder III + C-Al	Powder III + F-Al	Powder II + MA
Sintering curves	I	II	III	IV	II	II

C-Al, coarse Al powder (~ 20 μm); F-Al, fine Al powder (~ 2 μm); MA, master alloy powder (60 wt.% of Al and 40 wt.% of V)

changes happened during processing from TiH_2 (Powder II) to Ti-4V (Powder III). On the one hand, the dehydrogenation had completely finished, resulting in no TiH_2 peaks in the Ti-4V powder. On the other hand, the Ti-V solid solution had formed by self-propagating diffusion of Ti and V, resulting in no V peaks. Also, a small amount of the β phase in Ti-4V might be left upon cooling due to high levels of V, which acts as a β stabilizer.

Chemical composition of the powder was not tested, especially for interstitial elements, since it is hard to differentiate either N or O after air exposure. However, chemical analysis was performed for the as-sintered samples, shown in Table 3. O content in all samples is less than 0.2 wt.% (standard values for wrought Ti-6Al-4V in ASTM-B381) due to no contact with air in the experiment. Specifically, it can be seen that the O content increases with sintering temperature, except for the sample #3, which shows the same O content as sample #2. Fine Al powder in the sample #5 resulted in a sharp increase of O content compared to the sample #2, which may be related to Al_2O_3 film on the fine spherical Al powder particles. For the same reason, using the Al-V master alloy powder, instead of the element powder, may reduce the total amount of O content. Conversely, there is a slightly higher N content of 0.05 wt.% and not a clear trend for different samples. The reason for slightly higher N content may be associated with N_2 being used in the crushing machine and glove box as the shielding gas. In conclusion, chemical composition, especially interstitials, meets the standard values for wrought Ti-6Al-4V due to strict experimentation control. Thus, the total amount of interstitial elements would not significantly affect mechanical behavior of the sintered samples, which is of great importance for the BE PM Ti alloys.

3.2 Microstructure

Analysis was carried out to study microstructure and porosity evolution. Scanning electron microscopy (SEM) and optical microscopy (OM) images of different samples are presented in Fig. 4. The microstructure of samples #1-3 obtained from the same powder mixtures at different holding temperatures, is presented in Fig. 4(a-f). Sample #1, produced at 1050 °C, exhibits equiaxed or elongated α structures and intergranular β phase. The average α grain size is only 10 μm. When the temperature rises to 1150 °C, the microstructure is composed of lath-like α grains in different orientations and a small amount of $\alpha + \beta$ lamellae. As expected, the resulting microstructure of the sample #2 was quite similar to that obtained by HIP (Ref 28). Although the sintering temperature is higher than beta transus temperature of about 1000 °C for Ti-6Al-4V, the samples #1-2 do not have large-scale Widmanstätten microstructure. Such variation in microstructure appears to be associated with the sintering process. During sintering, more complicated processes, besides β phase transformation, have been completed, such as diffusion of Ti-Ti, Ti-Al, and Ti-V and coalescence, coarsening, and closure of pores. Before incomplete densification during sintering, pores and other defects hinder microstructure coarsening. Thus, only a small amount of parallel $\alpha + \beta$ Widmanstätten-like microstructure can be found in Fig. 4(a-d). An increase of the sintering temperature to 1250 °C changes the nature of the microcon-

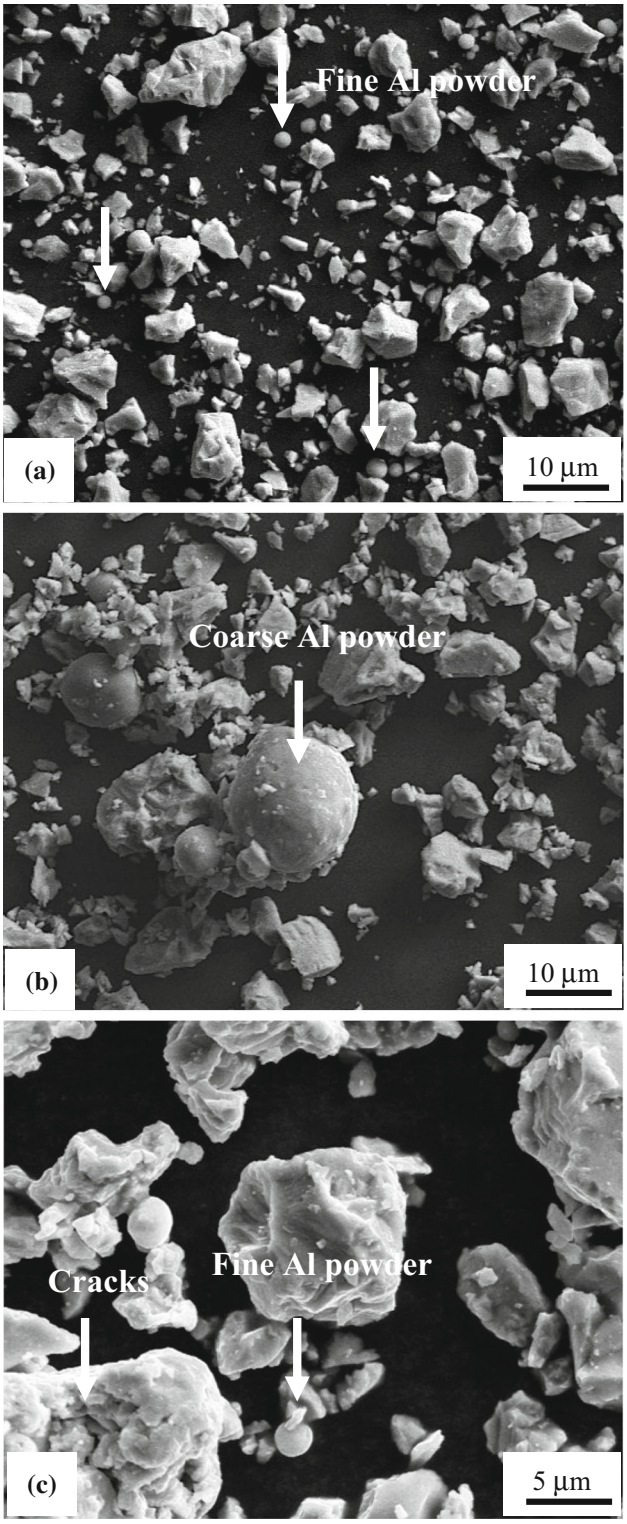

Fig. 2 Scanning electron micrographs of: (a, c) Ti-6Al-4V powder (Powder IV) with fine Al particles; (b) Ti-6Al-4V powder (Powder IV) with coarse Al particles

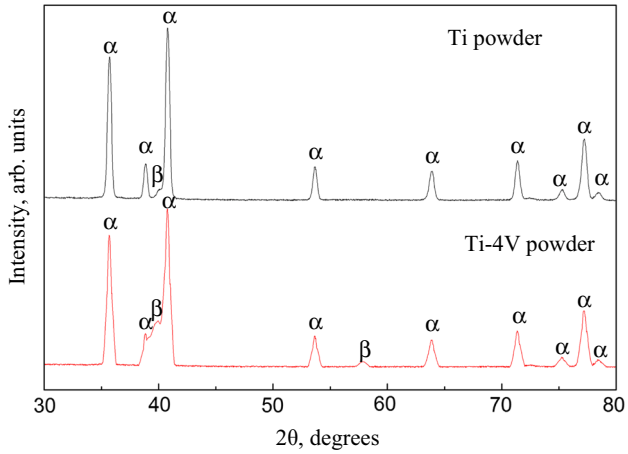

Fig. 3 X-ray diffraction patterns of pure Ti powder and Ti-4V powder

stituents. Typical Widmanstätten structure appeared, which contains coarse $\alpha + \beta$ colonies, with the 2-4 μm α lamellae thickness, and some grain boundary α phases. Another feature of the microstructure of the samples #1-3 is the residual porosity, which can be clearly identified in the SEM micrographs in Fig. 4(b, d, f). It is obvious that the rise of temperature results in the decrease of residual porosity. At 1050 °C, a considerable amount of pores can be seen in the matrix. The pore size distribution ranges between 1 μm and 10 μm. These small pores, interconnected and irregular in shape, indicate that the coalescence and coarsening processes have taken place. Sintering at 1150 °C leaves almost no visible pores in the microstructure, leading to relative density over 99.5%. Continuing to raise the sintering temperature to 1250 °C is not helpful for the improvement of density, but does induce grain coarsening.

As for samples #4-5, coarse Al powder and a slow heating rate were adopted to prove the effect of temporary liquid Al. The microstructure of the sample #4 is similar to the sample #2. However, large globular α phase and many pores were found, as denoted by the white circles and arrows in Fig. 4(g). The unusual phases seem to be formed due to the high levels of Al, which acts as the α stabilizer. Energy-dispersive spectra (EDS) analysis was carried out to further verify the inhomogeneous distribution of Al, with about 10 wt.% content. For the sample #5, the distinctive feature of microstructure is massive 1-2 μm pores. These pores may evolve from the void generation by the Kirkendall effect, which cannot be completely closed by sintering at 1150 °C. Some details about density are discussed in section 3.3.

In Fig. 4(k-l), the distinctly different acicular $\alpha + \beta$ lamellae region can clearly illustrate the inhomogeneous nature of the sample #6. It has been proven that V has a slower diffusion rate in β-Ti than in Al (Ref 29). Thus, V distribution is hindered by its combination with Al in the 60Al-40V MA powder, resulting in the V-rich region. High concentrations of the β-stabilizing alloying element V in the Ti matrix, near the alloying particles, result in a high stability of the β phase and prevent its decomposition upon cooling. The higher the concentration of the β stabilizer, the finer the $\alpha + \beta$ lamellae are formed. The EDS analysis indicates that the fine Widmanstätten microstructure has an elevated composition of V of approximately 15 wt.% V for the site 1 and 5.3 wt.% V for the site 2, as shown in Fig. 4(i). This is in agreement with other results (Ref 30, 31).

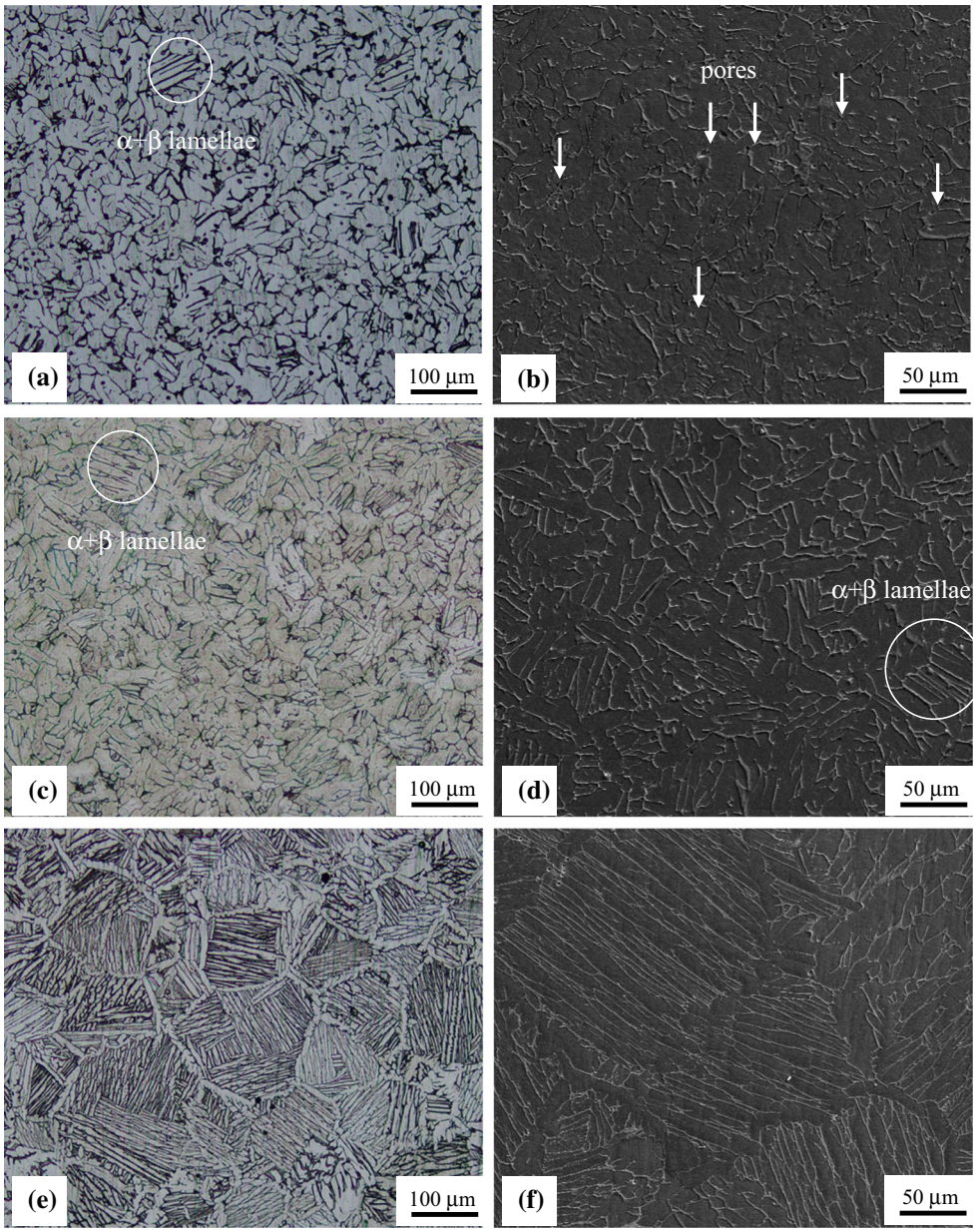

Fig. 4 Optical and scanning electron micrographs of as-sintered samples: (a, b) sample #1; (c, d) samples #2; (e, f) samples #3; (g, h) sample #4; (i, j) sample #5; (k, l) sample #6

3.3 Relative Density and Sintering

Porosity is the first issue for the PM Ti alloys, which significantly affects their mechanical properties. Previous research has shown that elevated sintering temperatures lead to higher relative density. In general, the temperature above 1300 °C for pressureless sintering can obtain full density, which results in distinct grain coarsening. In this study, sintering at 1150 °C can obtain a relative density of 99.5%, and there is no significant change at higher temperatures. This means 1150 °C is a suitable temperature for this processing route of Ti-6Al-4V PM. When adopting fine Al powder, or a slow heating process to 1150 °C, samples #4-5 show that relative density is less than 95%. As for sample #6, when Al and V are introduced by 60Al-40 V MA powder, the relative density is about 97%, which is lower than the sample #2.

It was found that the full density of Ti-6Al-4V obtained by vacuum sintering at a relatively low temperature (i.e., 1150 °C) may be attributed to temporary molten Al in the sintering process. To confirm the presence of instantaneous liquid Al formation during sintering, differential scanning calorimetry (DSC) was performed on compaction of Ti-6Al-4V fabricated with different particle sizes of Al powder. The DSC plot in Fig. 5(b) shows an endothermic peak at 680 °C, corresponding to the melting point of Al, which occurs endothermically at nearly 660 °C with 10.75 kJ/mol reaction energy. Nevertheless, the DSC plot in Fig. 5(a) exhibits no distinct endothermic peaks. This indicates that the emergence of molten Al in the Ti-6Al-4V BE powder sintering process requires special conditions, a fast heating rate under the melting point of Al and relatively large Al particle sizes. Otherwise, small amounts of

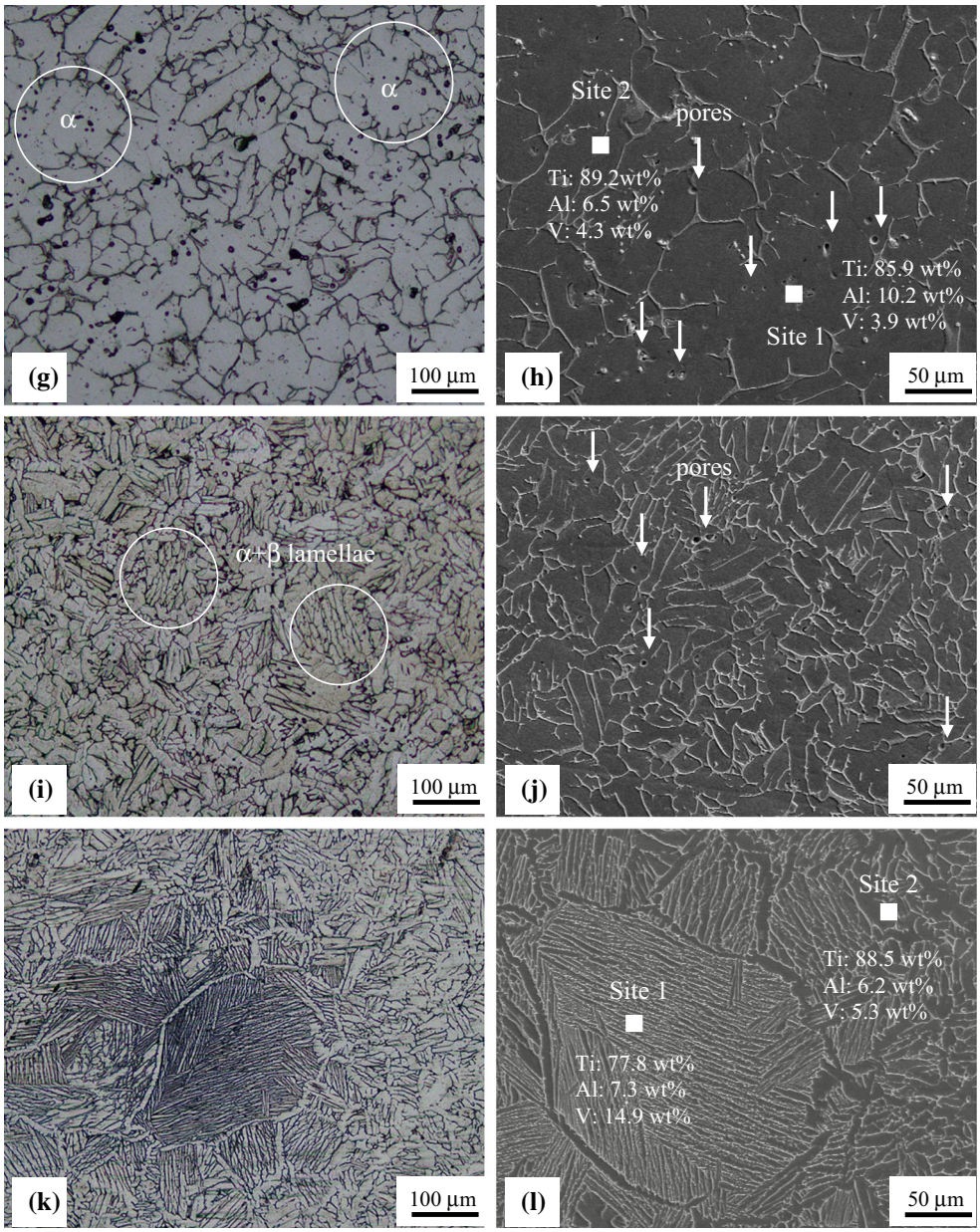

Fig. 4 continued

fine Al particles are prone to diffuse into the Ti particles in the solid state, resulting in no molten Al at sintering.

In order to further understand the mechanism of instantaneous molten Al in the vacuum sintering process, three compactions (#2, 5, and 6) were sintered at 750 °C for 10 min and then quenched in water. The backscattered electron (BSE) images are shown in Fig. 6, and the compositions measured by EDS at the noted points are listed in Table 4.

Microstructure of the sample #5 is shown in Fig. 6(a). Ti particles (light-colored areas) and their intergranular gaps are clearly seen, indicating no sintering neck formation. There is also a significant fraction of Al-rich areas (dark-colored areas). EDS results have proven that the dark area (site 1) predominantly contains 50.98 wt.% Al, 48.98 wt.% Ti and minimal V, while the center part of the Ti particle (site 3) has hardly any Al present. Relative density of this sample is about 81.3%, lower than compacts by cool isostatic pressing. Considerable swelling is caused by the Kirkendall effect while sintering. If subsequent sintering process cannot close these voids, massive pores will remain in the sintered sample #5.

However, microstructure of the sample #2 is distinctly different in Fig. 6(b). Coarse Al and quick heating rate form temporary molten Al before diffusion of Ti and Al particles. Once the temporary liquid phase has been formed, the sintering mechanism is quite different from the solid–solid diffusion, as shown in Fig. 7.

First, some physical changes are seen in the adjacent regions of the liquid phase. Molten Al flows into the gaps between the Ti particles, filling the pores, while smaller Ti particles are transferred to the molten Al region. Consequently, temporary liquid-phase sintering in this temperature range is more active compared to solid diffusion. Subsequently, the sintering

Table 3 Chemical composition (wt.%) of different Ti-6Al-4V samples

Sample	Ti	Al	V	Fe	C	H	O	N
#1	Bal.	5.94	4.02	0.154	0.014	0.017	0.15	0.065
#2	Bal.	6.12	4.22	0.168	0.014	0.012	0.17	0.069
#3	Bal.	5.84	4.2	0.162	0.012	0.003	0.17	0.057
#4	Bal.	6.13	3.9	0.163	0.012	0.003	0.15	0.06
#5	Bal.	5.98	4.21	0.135	0.013	0.012	0.22	0.054
#6	Bal.	6.06	3.96	0.124	0.015	0.007	0.13	0.039
Grade-F5 ASTM-B381	Bal.	5.5-6.75	3.5-4.5	0.4	0.08	0.015	0.2	0.05

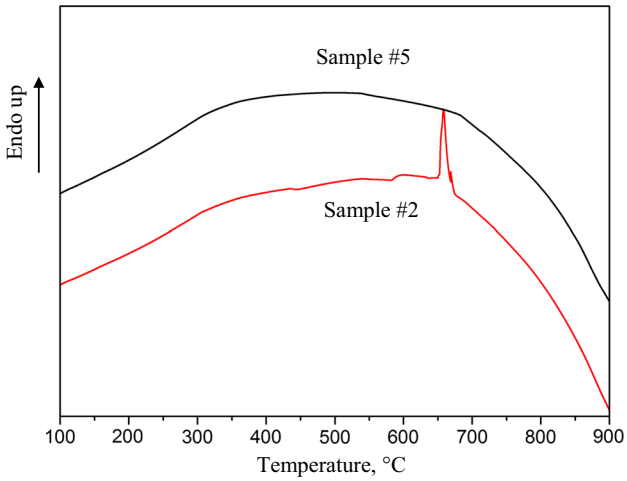

Fig. 5 DSC curves of Ti-6Al-4V compacts (samples #2 and #5) during heating to 900 °C at 10 °C/min

mechanism was changed due to the formation of molten Al. It is widely believed that Al is the only diffusing component in diffusion couples (Ref 32), because of the greater diffusion rate from Al into Ti than from Ti into Al. Currently, an increasing number of studies have found that the reaction mechanism between Ti and Al is significantly different below and above the melting point of Al. At temperatures below the melting point of aluminum of 400-660 °C, Ti and Al are both present as solid phases. Therefore, the reaction between them is the process of solids dissolution, which is controlled by diffusion (Ref 33, 34). It is easy to understand that diffusion of Al prior to Ti is due to the large difference of solid solubility between them. The solubility of Al in Ti is approximately 11.7 at.%, whereas the maximum solubility of Ti in Al is approximately only 0.12 at.% in the 500-650 °C range (Ref 35). With temperatures above 700 °C, there are continuous liquid Al phases present. Many studies have shown that Ti is the main diffusing species instead of Al in these circumstances (Ref 36, 37). When liquid Al is involved in the reaction, Ti_3Al may form even at very low Al compositions. $TiAl_3$ phase is generally believed to be the only primary phase in the Ti/Al interface zones (Ref 38), which continuously generates in the form of spherical particles. These intermetallic phases are then ejected into the liquid Al by the surface force, allowing new reaction interfaces to be generated until Al is consumed. In other words, the element migration in the solid phase is dominated by grain boundary diffusion with low activation energy. When liquid phase appears, the reaction-controlled process is characterized by high activation energy. From Fig. 6(b), there are no obvious

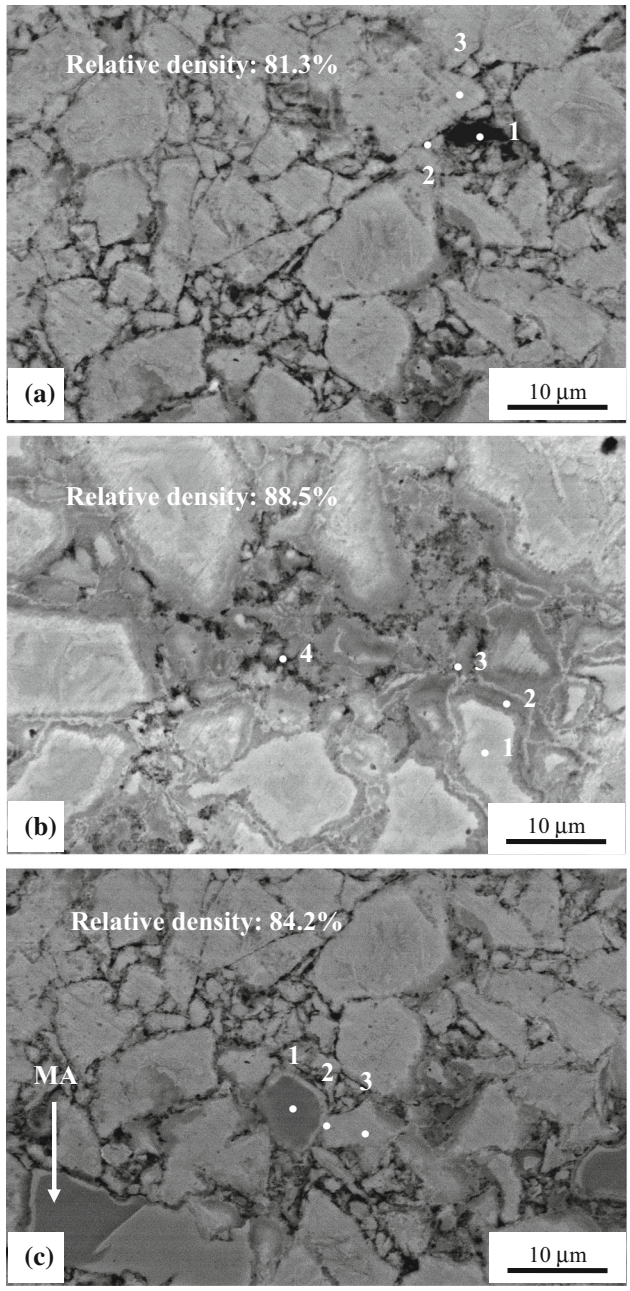

Fig. 6 SEM BSE images of quenched specimens sintered at 750 °C for 10 min: (a) sample #5; (b) sample #2; (c) sample #6

Table 4 EDS chemical analysis results (wt.%) for different samples sintering at 750 °C from Fig. 6

Sample	Element	Site 1	Site 2	Site 3	Site 4
#2 (Fig. 6a)	Ti	48.98	85.07	95.99	
	Al	50.98	10.75	0.12	
	V	0.04	4.18	3.89	
#5 (Fig. 6b)	Ti	96.05	84.95	84.06	54.97
	Al	0.09	11.40	12.44	44.91
	V	3.86	3.65	3.50	0.12
#6 (Fig. 6c)	Ti	0.31	97.62	99.96	…
	Al	58.92	2.38	0.04	…
	V	40.77	0.00	0.00	…

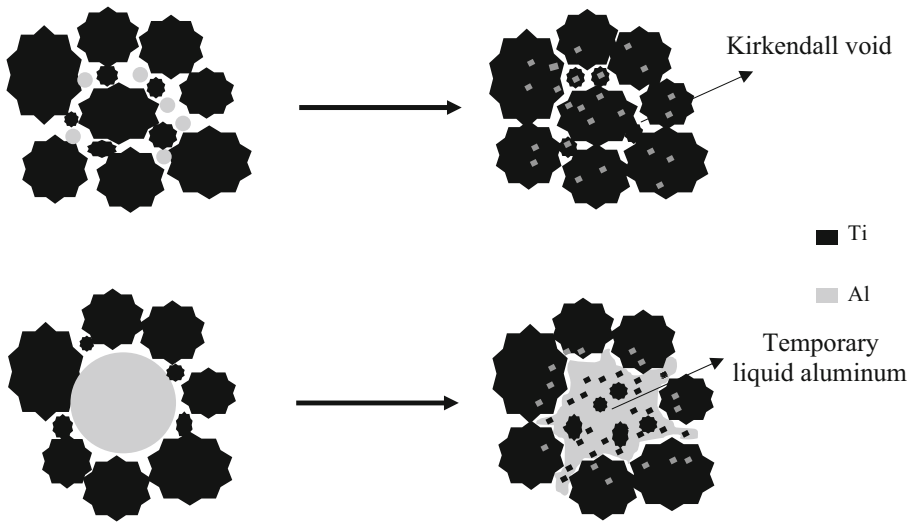

Fig. 7 Schematic diagram of solid-phase sintering and temporary liquid-phase sintering

gaps between Ti particles, replaced by gray Ti-Al solid solution phase (site 2), which gradually translates into sintering neck in continuing heating process.

In Fig. 6(c), the master alloy (MA particles, site 1) has maintained a composition close to the original composition. The nearby area of the Ti matrix (site 2) shows a small uptake of Al, with no V, while the area far from the MA particles in Ti matrix (site 3) has maintained nearly pure Ti composition. These results indicate that solid-state diffusion process of MA particles is slow at 750 °C. On the other hand, it is observed that Al diffuses through the Ti matrix at a faster rate than V, resulting in no V in Ti particles. This phenomenon is consistent with previous work, which leads to the fine Widmanstätten microstructure, as shown in Fig. 4(k, l) by interlocked Al and V into the residual particle. Compared with sample #5, the Kirkendall effect is weakened by the use of Al-V master alloy instead of pure Al powder. Thus, a slight increase in relative density is probably related to sintering between Ti powder particles.

3.4 Mechanical Properties

The tensile strength and elongation of six samples are summarized in Table 5. For the samples #1-2, it is clear that the ultimate tensile strength and yield stress are both increasing gradually due to the higher relative density at elevated temperatures. However, for the samples #2-3, completely different microstructure may account for the strength. The microstructure transformed from equiaxed and elongated α structures to finer lamellar structure, with a smaller α colony size (the width of individual α plates), which is the most important microstructure parameter determining mechanical properties. With decreasing α colony size, the strength is improved (39), which may be the main reason for the strength increase. In addition, elongation also varies with the relative density and microstructure transformation. When sintered at 1150 °C, fine microstructure and optimal comprehensive mechanical properties (UTS = 935 MPa, Y.S. = 865 MPa, EL. = 15.8%) are obtained.

Fractographic analysis of the tensile test specimens by SEM was carried out, and the results are presented in Fig. 8. The equiaxed and slightly elongated α structures (samples #1-2) show typical transgranular ductile dimpled rupture with abundant equiaxed dimples. The size of the dimples found in the sample #2 seems to be larger than the sample #3. The surface of sample #3 contains brittle transgranular fractures and cleavage, which resulted from the formation of a long river pattern. This pattern appears to be related to long and straight α phase with similar crystallographic orientations in the Widmanstätten microstructure. This fracture mode during tensile failure tends to sharply reduce ductility. For the sample #4, cracking is characterized by fan-shaped flat transgranular

Table 5 Effect of the sintering process and powder type on the tensile properties of different PM Ti-6Al-4V samples

Sample number	Relative density, %	Mechanical properties			
		UTS, MPa	Y.S., MPa	El., %	R, %
#1	96.5 ± 0.5	874 ± 5	823 ± 3	7.2 ± 1.3	5.3 ± 2.5
#2	99.5 ± 0.2	935 ± 5	865 ± 4	15.8 ± 0.7	35.6 ± 1.2
#3	99.7 ± 0.2	1008 ± 13	921 ± 5	3.4 ± 0.8	…
#4	95.1 ± 0.5	912 ± 3	856 ± 6	1-4	…
#5	94.3 ± 0.7	830 ± 26	…	2.2 ± 0.4	…
#6	97.3 ± 0.3	950 ± 16	887 ± 4	2-4	…
Wrought ASTMB381	100	825	895	10	25

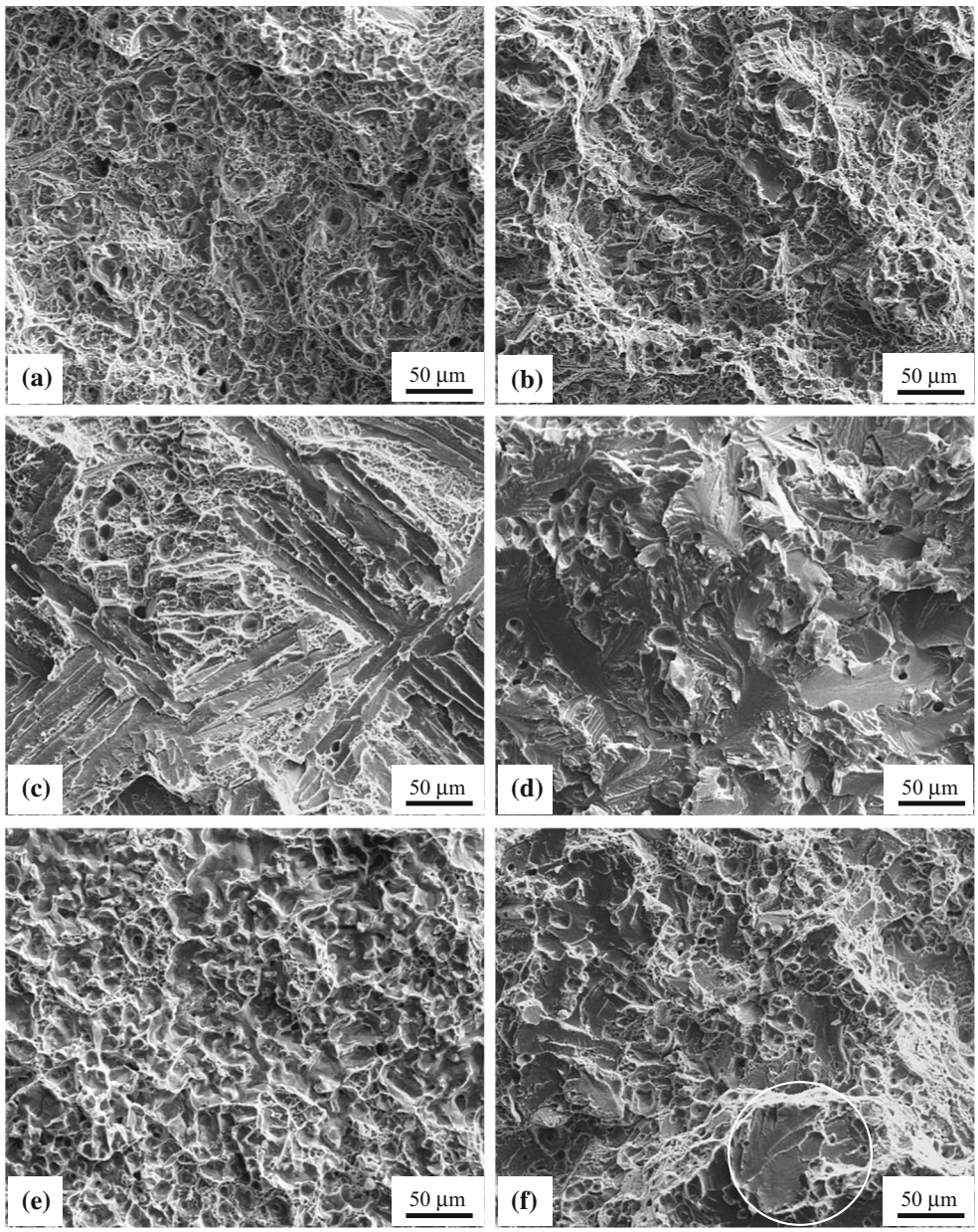

Fig. 8 Scanning electron fractographs of the specimens after tensile failure: (a) sample #1; (b) sample #2; (c) sample #3; (d) sample #4; (e) sample #5; (f) sample #6

facets, which are on the scale of the coarser equiaxed α colonies in this sample, as shown in Fig. 4(g). Sample #5 resulted in predominant cleavage fracture, with little evidence of dimples due to so many micropores in the matrix. Sample #6 has combined ductile and brittle fracture mode with a number of dimples seen across the fracture surface. In addition, distinct

transgranular facets may be related to microstructure inhomogeneities, an acicular α/β lamellae region, which can lead to substantial ductility decrease.

4. Conclusions

Microstructure, density and mechanical properties of six as-sintered Ti-6Al-4V samples with different powder mixtures and sintering profiles were characterized. The following conclusions can be drawn:

1. PM Ti-6Al-4V alloy with 99.5% relative density and comprehensive mechanical properties (UTS = 935 MPa, Y.S. = 865 MPa, El = 15.8%) was successfully manufactured by vacuum pressureless sintering at 1150 °C. The as-sintered materials have fine homogeneous basket-weave microstructure and low oxygen content (0.17 wt.%).
2. Investigation of different as-sintered samples revealed that higher density can be obtained by generating transient molten Al at the sintering process, instead of increasing the sintering temperature. The presence of temporary liquid phase changes from diffusion process to reaction process. It also accelerates the sintering neck formation and short-range motion of ultrafine particles, improving sinterability of powder mixtures. The coarse Al powder and a rapid heating rate under the melting point of Al contribute to molten Al formation.

References

1. R.R. Boyer, An Overview on the Use of Titanium in the Aerospace Industry, *Mater. Sci. Eng. A*, 1996, **213**(1–2), p 103–114
2. Z. Esen and Ş. Bor, Characterization of Ti-6Al-4V Alloy Foams Synthesized by Space Holder Technique, *Mater. Sci. Eng. A*, 2011, **528**(7–8), p 3200–3209
3. Z.Z. Fang and P. Sun, Pathways to Optimize Performance/Cost Ratio of Powder Metallurgy Titanium—A Perspective, *Key Eng. Mater.*, 2012, **520**, p 15–23
4. D. Banerjee and J.C. Williams, Perspectives on Titanium Science and Technology, *Acta Mater.*, 2013, **61**(3), p 844–879
5. T.E. Norgate and G. Wellwood, The Potential Applications for Titanium Metal Powder and their Life Cycle Impacts, *JOM*, 2006, **58**(9), p 58–63
6. M.A. Imam and F.H. Froes, Low Cost Titanium and Developing Applications, *JOM*, 2010, **62**(5), p 17–20
7. S.J. Mashl, J.C. Hebeisen, and C.G. Hjorth, Producing Large P/M Near-net Shapes Using Hot Isostatic Pressing, *JOM*, 1999, **51**(7), p 29–31
8. O.M. Ivasishin, D.G. Savvakin, F. Froes, V.C. Mokson, and K.A. Bondareva, Synthesis of Alloy Ti-6Al-4V with Low Residual Porosity by a Powder Metallurgy Method, *Powder Metall. Met.*, 2002, **41**(7–8), p 382–390
9. C.C. Chen, Recent Advancement in Titanium Near-Net-Shape Technology, *JOM*, 1982, **34**(11), p 30–35
10. H. Wang, Z.Z. Fang, and P. Sun, A Critical Review of Mechanical Properties of Powder Metallurgy Titanium, *Int. J. Powder Metall.*, 2010, **46**(5), p 45–57
11. Y. Kim, E.P. Kim, and Y.B. Song, Microstructure and Mechanical Properties of Hot Isostatically Pressed Ti-6Al-4V Alloy, *J. Alloy. Compd.*, 2014, **603**(8), p 207–212
12. L. Xu, R. Guo, and C. Bai, Effect of Hot Isostatic Pressing Conditions and Cooling Rate on Microstructure and Properties of Ti-6Al-4V Alloy from Atomized Powder, *J. Mater. Sci. Technol.*, 2014, **30**(12), p 1289–1295
13. F. Yang, D. Zhang, and B. Gabbitas, Microstructural Evolution during Extrusion of a Ti/Al/Al35V65 (Ti-6Al-4V) Powder Compact and the Mechanical Properties of the Extruded Rod, *Mater. Sci. Eng. A*, 2014, **598**, p 360–367
14. C. Liang, M.X. Ma, and M.T. Jia, Microstructures and Tensile Mechanical Properties of Ti-6Al-4V Bar/Disk Fabricated by Powder Compact Extrusion/Forging, *Mater. Sci. Eng. A*, 2014, **619**, p 290–299
15. D. Zhang, S. Raynova, and V. Nadakuduru, Consolidation of Titanium, and Ti-6Al-4V Alloy Powders by Powder Compact Forging, *Mater. Sci. Forum*, 2009, **618–619**, p 513–516
16. J.F. Lu, Z.H. Zhang, and Z.F. Liu, Sintering Mechanism of Ti-6Al-4V Prepared by SPS, *AMM*, 2015, **782**, p 97–101
17. Y. Yamamoto, J.O. Kiggans, and M.B. Clark, Consolidation Process in Near Net Shape Manufacturing of Armstrong CP-Ti/Ti-6Al-4V Powders, *Key Eng. Mater.*, 2010, **436**, p 103–111
18. L. Bolzoni, E.M. Ruiz-Navas, and E. Gordo, Feasibility Study of the Production of Biomedical Ti-6Al-4V Alloy by Powder Metallurgy, *Mater. Sci. Eng. C*, 2015, **49**(3), p 400–407
19. J.D. Paramore, Z.Z. Fang, P. Sun, M. Koopman, K.S.R. Chandran, and M. Dunstan, A Powder Metallurgy Method for Manufacturing Ti-6Al-4V with Wrought-Like Microstructures and Mechanical Properties via Hydrogen Sintering and Phase Transformation (HSPT), *Scr. Mater.*, 2015, **107**, p 103–106
20. C. Haase, R. Lapovok, H.P. Ng, and Y. Estrin, Production of Ti-6Al-4V Billet Through Compaction of Blended Elemental Powders by Equal-Channel Angular Pressing, *Mater. Sci. Eng. A*, 2012, **550**, p 263–272
21. H.P. Ng, C. Haase, R. Lapovok, and Y. Estrin, Improving Sinterability of Ti–6Al–4V from Blended Elemental Powders through Equal Channel Angular Pressing, *Mater. Sci. Eng. A*, 2013, **565**(3), p 396–404
22. T. Fujita, A. Ogawa, C. Ouchi, and H. Tajima, Microstructure and Properties of Titanium Alloy Produced in the Newly Developed Blended Elemental Powder Metallurgy Process, *Mater. Sci. Eng. A*, 1996, **213**(1–2), p 148–153
23. W. Chen, Y. Yamamoto, W.H. Peter, M.B. Clark, S.D. Nunn, and J.O. Kiggans, The Investigation of Die-pressing and Sintering Behavior of ITP CP-Ti and Ti-6Al-4V Powders, *J. Alloy. Compd.*, 2012, **541**, p 440–447
24. X. Xu and P. Nash, Sintering Mechanisms of Armstrong Prealloyed Ti-6Al-4V Powders, *Mater. Sci. Eng. A*, 2014, **607**, p 409–416
25. I.M. Robertson and G.B. Schaffer, Swelling During Sintering of Titanium Alloys Based on Titanium Hydride Powder, *Powder Metall.*, 2010, **53**(1), p 27–33
26. H.T. Wang, M. Lefler, Z.Z. Fang, T. Lei, and J.M. Zhang, Titanium and Titanium Alloy via Sintering of TiH_2, *Key Eng. Mater.*, 2010, **436**, p 157–163
27. J.E. Smugeresky and D.B. Dawson, New Titanium Alloys for Blended Elemental Powder Processing, *Powder Metall.*, 1981, **30**(1), p 87–94
28. R. Guo, L. Xu, J. Wu, and B.Y. Zong, Microstructural Evolution and Mechanical Properties of Powder Metallurgy Ti–6Al–4V Alloy Based on Heat Response, *Mater. Sci. Eng. A*, 2015, **639**, p 327–334
29. Y.F. Yang, S.D. Luo, G.B. Schaffer, and M. Qian, Sintering of Ti-10V-2Fe-3Al and Mechanical Properties, *Mater. Sci. Eng. A*, 2011, **528**(22–23), p 6719–6726
30. G. Steedman and S.F. Corbin, Determining Sintering Mechanisms and Rate of In Situ Homogenisation during Master Alloy Sintering of Ti-6Al-4V, *Powder Metall.*, 2015, **58**(1), p 67–80
31. A. Carman, L.C. Zhang, O.M. Ivasishin, and E.V. Pereloma, Role of Alloying Elements in Microstructure Evolution and Alloying Elements Behaviour during Sintering of a Near-β Titanium Alloy, *Mater. Sci. Eng. A*, 2011, **528**(3), p 1686–1693
32. F.J.J. van Loo and G.D. Rieck, Diffusion in the Titanium-Aluminium System-I. Interdiffusion Between Solid Al and Ti or Ti-Al Alloys, *Acta Metall.*, 1973, **21**, p 61–71
33. Y. Mishin and C. Herzig, Diffusion in the Ti-Al System, *Acta Mater.*, 2000, **48**(3), p 589–623
34. M. Thuillard, L.T. Tran, and M.A. Nicolet, Al_3Ti Formation by Diffusion of Aluminum Through Titanium, *Thin Solid Films*, 1988, **166**, p 21–27
35. H.W. Kerr, J. Cisse, and G.F. Bolling, On Equilibrium and Non-Equilibrium Peritectic Transformations, *Acta Metall.*, 1974, **22**(6), p 677–686

36. D.J. Harach and K.S. Vecchio, Microstructure Evolution in Metal-Intermetallic Laminate (mil) Composites Synthesized by Reactive Foil Sintering in Air, *Metall. Mater. Trans. A*, 2001, **32**(6), p 1493–1505
37. W.Y. Yang and G.C. Weatherly, A Study of Combustion Synthesis of Ti-Al Intermetallic Compounds, *J. Mater. Sci.*, 1996, **31**(14), p 3707–3713
38. L. Xu, Y.Y. Cui, Y.L. Hao, and R. Yang, Growth of Intermetallic Layer in Multi-laminated Ti/Al Diffusion Couples, *Mater. Sci. Eng. A*, 2006, **435–436**(4), p 638–647
39. G. Lütjering, Influence of Processing on Microstructure and Mechanical Properties of ($\alpha + \beta$) Titanium Alloys, *Mater. Sci. Eng. A*, 1998, **243**(1–2), p 32–45